Green Chemistry

PAPER

View Article Online
View Journal | View Issue

Cite this: *Green Chem.*, 2017, **19**, 4879

A new selective route towards benzoic acid and derivatives from biomass-derived coumalic acid†

Toni Pfennig, [a,b] Jack M. Carraher, [a,b] Ashwin Chemburkar, [b,c] Robert L. Johnson, [a,b] Austin T. Anderson, [a,b] Jean-Philippe Tessonnier, [a,b] Matthew Neurock [b,c] and Brent H. Shanks *[a,b]

The selective production of aromatics from bio-based sources is an area of interest to expand the potential for greener alternatives to petroleum-derived chemicals. A scalable, efficient route to produce bio-based benzoates is demonstrated by carrying out heterogeneous catalytic reactions in non-toxic bio-based solvents at 180 °C obtaining yields of up to 100 mol%. This approach extends the 2-pyrone (coumalic acid/methyl coumalate) Diels–Alder platform by utilizing a bioavailable co-reactant ethylene. A detailed investigation using a combination of kinetic experiments, DFT calculations, and multi-dimensional NMR was carried out to determine the detailed reaction network, and the corresponding activation energies for critical steps. Additionally, a series of experiments were conducted to maximize the yields by comparing different solvents, for both coumalic acid and methyl coumalate. Our results show that the choice of solvent was a significant factor when coumalic acid was the reactant (yields 71–92 mol%), while methyl coumalate was only minimally affected by the solvent (yields 95–100 mol%). Interestingly, the reaction network and kinetic analysis showed that the Diels–Alder reactions were not significantly different between coumalic acid and methyl coumalate, with the rate limiting step for both being decarboxylation with an activation barrier of 141 kJ mol^{-1} compared to 77 kJ mol^{-1} for the formation of the bicyclic adduct. Finally, the reaction cascade was found to be highly susceptible to by-product formation when as little as 5 vol% water was present in the solvent, which demonstrates that the absence of water is essential for high yielding benzoate production.

Received 6th July 2017,
Accepted 31st August 2017

DOI: 10.1039/c7gc02041d

rsc.li/greenchem

Introduction

The search for alternatives to fossil-based feedstocks has led to rapid technological advances in the field of bio-renewable chemicals creating many potential opportunities for materials based on renewable carbon sources.[1–6] Technologies to produce aromatics from biomass-derived sources have become targets of interest due to the expansion of shale gas extraction, which has led to a relatively reduced availability of >C4 building blocks, including aromatics.[2,6,7] Aromatics are among the most important building blocks used by the chemical industry for the production of a wide array of products, so there is an incentive for the development of selective processes to produce aromatics from bio-based feedstocks.[2,6,7]

Benzoic acid (BA) is a large scale commodity chemical with an annual production of 638 kt[8] currently produced by the partial oxidation of toluene using a cobalt–manganese catalyst. BA is used in a wide variety of applications including plasticizers, preservatives, dyes/perfumes and as a feed to produce other chemicals including phenol, caprolactam, and benzaldehyde. Hence, a renewable pathway to produce BA would have broad ranging impacts throughout the chemical value chain.

One route to make bio-based BA is through a formic acid mediated dehydration of quinic or shikimic acid produced *via* fermentation. This process has several desirable features including high yields for the chemical transformation of quinic and shikimic acids into benzoic acid (up to 90%)[2] and high titers up to 60 g L^{-1} for quinic acid and 71 g L^{-1} shikimic acid starting from the substrate glucose and using metabolically engineered *E. coli*.[9,10] However, the primary drawback of this approach is the intrinsically low maximum theoretical yield of the shikimic/quinic acid fermentation of 43%, and to date the highest yields reported correspond to an overall

[a]*Department of Chemical and Biological Engineering, Iowa State University, Ames, IA 50011, USA. E-mail: bshanks@iastate.edu*
[b]*NSF Engineering Research Center for Biorenewable Chemicals (CBiRC), Ames, IA 50011, USA*
[c]*Department of Chemical Engineering and Material Science, University of Minnesota, Minneapolis, MN 55455, USA*
†Electronic supplementary information (ESI) available. See DOI: 10.1039/c7gc02041d

mol/mol yield of 23 and 27%.[10] This fermentation bottleneck creates a significant problem for efficient utilization of the glucose feedstock. As a major fraction of the total cost of the fermentation step is the glucose feedstock, its inefficient utilization would have a significant negative impact on the cost required to produce BA.

An alternative pathway to bio-based BA and its methyl ester (MeBA) is through a furanic based platform utilizing a Diels–Alder reaction sequence of furan with methyl acrylate (or acrylic acid) showing moderate yields of up to 51 mol%.[7] Additionally Diels–Alder reactions of methyl furan with ethylene provide a viable pathway to produce bio-based toluene, which could be utilized as a drop-in replacement for the production of BA. Toluene selectivities, however, never exceeded 46 mol% due to by-product formation.[11] Improvement of this selectivity would require approaches to improve the stability of bio-based starting materials, thereby minimizing by-product formation.

Another approach utilizing biological and chemical catalysis to produce partially biomass-derived methyl benzoate (MeBA) is based on the bio-based cyclic lactone methyl coumalate (MeCMA). The formation of bio-based MeBA is accomplished using a one-pot Diels–Alder/decarboxylation/dehydrogenation reaction sequence between MeCMA and butyl vinyl ether with excellent yields of up to 89 mol%.[12]

Bio-based 2-pyrones can be produced from the fermentation of glucose to form malic acid[13,14] followed by acid catalyzed dimerization of malic acid to coumalic acid (Scheme 1).[12] The synthesis of 2-pyrone coumalic acid (CMA) *via* this route has several attractive features. First, the atom efficiency of the malic acid fermentation is highly favorable, with the capability to even utilize a CO_2 fixating pathway allowing for a theoretical yield of 2 moles of malate per mole of glucose (Scheme 1).[14] Second, efficient fermentation technology has already been developed for this route. For example, Novozymes currently uses a metabolically engineered *Aspergillus oryzae* capable of producing 1.38 mol malate per mol glucose with a theoretical yield of 69% and with high titers of 154 g L^{-1}, which could be implemented on an industrial scale.[13]

An approach to improve the viability of the 2-pyrone CMA/MeCMA platform is to utilize a less expensive dienophile as the co-reactant. In theory ethylene should work in an analogous fashion to butyl vinyl ether, but at a substantially lower cost with nearly perfect atom efficiency. Additionally, as the production of ethylene from bio-ethanol is commercially demonstrated, a 100% bio-based process is potentially possible.[3]

As part of the development of new biomass-derived and renewable processes, we herein report on the synthesis of BA or MeBA from CMA or MeCMA, respectively, and ethylene with very high yields of >91 mol% utilizing a one-pot sequential Diels–Alder/decarboxylation/dehydrogenation reaction path. Considering the industrial importance of renewable BA, and the lack of available comprehensive information about this alternative route in the literature, the focus of this work is to provide detailed information of the reaction network, and intrinsic kinetics of individual reaction steps, which can be used to improve the overall process.

Results and discussion

The formation of benzoic acid from coumalic acid

Experiments were conducted to examine the BA and MeBA yields obtained in several solvents using either CMA or MeCMA, respectively. The reaction between CMA and ethylene in a non-polar solvent, toluene, resulted in 71 mol% yield of BA at 100 mol% CMA conversion (Table 1, entry 1). This outcome was similar to the reported yields (76%) for the Diels–Alder reaction of CMA with propylene in toluene,[15,16] which was thought to be due to CMA being sparingly soluble in toluene leading to a substantial amount of CMA being converted to unidentified by-products. Therefore, a solvent was used to increase the solubility of CMA in order to improve the overall reaction yield. We have previously shown that γ-valerolactone (GVL) is a good polar aprotic solvent for this reaction system due to structural similarities.[16] The use of GVL resulted in only a slightly higher BA yield of 76 mol% (Table 1, entry 2 and Fig. S1†). Still, a considerable amount (~24 mol%) of the initial CMA was lost to by-product formation. Results from previous studies suggested that CMA stability was limited in GVL under the reaction conditions due to the presence of residual water in GVL.[16] This hypothesis was tested by using polar aprotic solvents, 1,4-dioxane or acetone, resulting in a significant improvement in the BA yield (Table 1, entries 3 and 7). The reaction profile of the CMA consumption over time is displayed in Fig. S2.† At 100 mol% CMA conversion the BA selectivity was 91 mol% after a 4 h reaction at 180 °C for both solvents. From UPLC-PDA/QDa analysis, it was evident that small amounts of **4** and **6** (see Scheme 2) were present. Additionally, the formation of **4** was verified by NMR analysis showing that roughly 6 mol% of **4** was formed (Table 1, entry 3). At this reaction temperature, the dehydrogenation reaction was extremely rapid as evident from the lack of an observable amount of the diene intermediate (**3**). This result was consistent

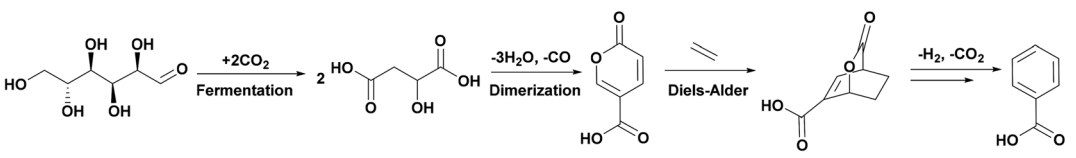

Scheme 1 The formation of benzoic acid starting from glucose fermentation to malic acid using acid catalysed dimerization to coumalic acid followed by a Diels–Alder/decarboxylation/dehydrogenation reaction sequence to yield the desired aromatics.

Table 1 Conversion of CMA/MeCMA with ethylene to BA/MeBA

Entry	Reactant	Solvent	Conv. (1) [mol%]	Selectivity (5) [mol%]	(3) [mol%]	(4) [mol%]	(6) [mol%]
1	CMA	Toluene	100	71	[a]	[a]	[a]
2	CMA	GVL	100	76	[a]	[a]	[a]
3	CMA	1,4-Dioxane	100	91 ± 1.5	[a]	5.8[d]	[a]
4	MeCMA	Toluene	100	100 ± 2	[b]	[b]	7 ± 2[c]
5	MeCMA	GVL	100	99 ± 1	[b]	[b]	2 ± 10[c]
6	MeCMA	1,4-Dioxane	100	95 ± 1	2 ± 7[c]	2 ± 3[c]	5 ± 8[c]
7	CMA	Acetone	100	91	[a]	[a]	[a]

Reaction conditions: Temperature: 180 °C, reaction time: 4 h, starting concentration: 10 mg ml^{-1} MeCMA/CMA (1) in 1,4-dioxane, reaction volume: 30 ml, pressure: 500 psig ethylene, agitation: 400 rpm, and Pd/C catalyst: 100 mg. [a] Unable to quantify by-products with UPLC-PDA/QDa. [b] By-products not detected with GC-FID/MS. [c] Cyclohexadiene (3) and cyclohexene (6) intermediates were quantified based on methyl benzoate (5) as reference due to a similar FID response factor. Double Diels–Alder by-product (4) was approximated using methyl benzoate (5) as the reference material. [d] Quantified *via* ^{1}H-NMR.

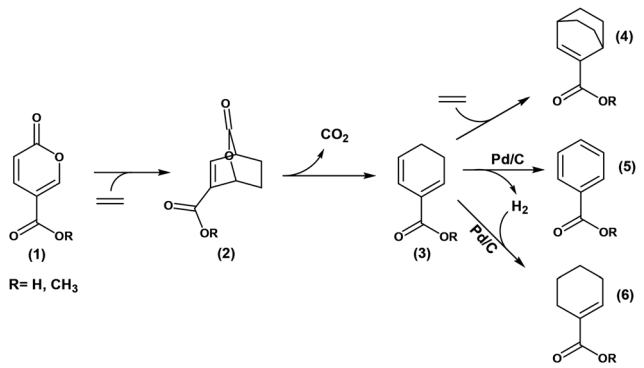

Scheme 2 Network for the reaction of CMA/MeCMA with ethylene.

with previous studies[16] in which we have shown that the dehydrogenation of the diene species proceeded significantly faster than the decarboxylation of the bicyclic intermediate, thereby suggesting that the decarboxylation of the cycloadduct was the limiting step in the reaction network.[16] Kinetic studies and DFT calculations corroborate that decarboxylation is the rate limiting step, which will be discussed in the subsequent sections.

Literature reports suggest that changing the functional group on the starting substrate could significantly influence the stability and reactivity towards Diels–Alder reactions.[15,17,18] This effect was demonstrated by Pacheco *et al.* using furanic dienes showing different product selectivities when various oxidized versions of HMF were made to react with ethylene, which was expected to be the outcome of different functionalities of the oxygenated furans.[17] Furthermore, Bérard *et al.* observed that the reaction of sorbic acid with ethylene resulted in only low conversion (3%), while using the ethyl ester of sorbic acid instead, afforded an ~5 fold increase in conversion (14%).[18] A similar phenomenon was also observed with 2-pyrones showing improved yields when MeCMA instead of CMA reacts with propylene.[15]

Therefore, reactions were also performed using MeCMA as the reactant to determine if starting with the methyl ester of CMA (MeCMA) would alter the reaction. Interestingly, the reaction in toluene showed a tremendous improvement in yield with 100 mol% selectivity after complete conversion (Table 1, entry 4 and Fig. S3†). The higher selectivity with MeCMA was also consistent with the hypothesis of the importance of the solubility of the starting substrate in the 2-pyrone conversion. Similarly, when the polar aprotic solvent GVL was used to mediate the MeCMA and ethylene reaction, a conversion of 100 mol% with nearly 100 mol% MeBA selectivity (Table 1, entry 5 and Fig. S4†) was achieved. As the CMA conversion in GVL only resulted in a selectivity of 76 mol% (Table 1, entry 2 and Fig. S1†), the esterification of the carboxylate moiety likely played a significant role in improving the selectivity. Since CMA conversion to BA achieved the highest selectivity in 1,4-dioxane, we also performed the MeCMA conversion in 1,4-dioxane. As shown in Table 1, entry 6 reported only a slightly better product selectivity (95 mol%) compared to CMA (91 mol%). The GC-MS analysis suggested that the remaining five percent was attributed to the unreacted methyl cyclohexa-1,5-diene carboxylate intermediate (3), the formation of methyl cyclohex-1-ene carboxylate (6), and the double Diels–Alder (DDA) by-product (4), which was believed to be the outcome of a consecutive Diels–Alder reaction of 3 with ethylene (Scheme 2). The concentration profiles of 1, 2, 3, 4, 5 and 6 over time are displayed in Fig. S17.† The formation of 2, 3, and 6 was validated *via* 2D-NMR COSY and HSQC experiments (see Fig. S1–S11†) and will be explained in detail in the following section.

Elucidating the reaction network

To elucidate where by-product formation was occurring, experiments were performed to determine the reaction network. Given the extensive work on Diels–Alder reactions of 2-pyrones[12,19–29] a reaction network was postulated, which is depicted in Scheme 2. The reaction of CMA/MeCMA with ethylene follows a series of reactions that include Diels–Alder adduct formation (2), decarboxylation of the adduct to yield 3 and a Pd/C catalysed dehydrogenation reaction to form the desired aromatics (5). In the presence of the Pd/C catalyst, additional minor products (4) and (6) were observed (Table 1,

entry 6). The formation of **6** is likely the result of a Pd catalysed hydrogenation of **3**. The hydrogen needed for this step was likely formed through the dehydrogenation of **3** to **5**. Data shown in Fig. S5† support the proposed reaction network which is evident *via* the clear trend showing how the conversion of **1** resulted in the formation of intermediates (**2**) and (**3**) and small amounts (<8 mol%) of **4** and **6** while **5** was formed. The structural identification of the intermediates (**2**) and (**3**) and by-products (**4**) was determined by performing 1D and 2D NMR experiments of the reaction products from the MeCMA reaction with ethylene in the absence of a catalyst to examine the Diels–Alder/decarboxylation sequence (see Fig. S6–S16 and Tables S1–S3†). These analyses confirmed the formation of **2**, **3** and **4**. Without the catalyst, the by-product (**6**) was not observed. Therefore, it appeared that the formation of **6** was only realized when there was formation of hydrogen from dehydrogenation of **4** to **5**. Similar observations were made when CMA was used as the starting substrate.

2-Pyrone degradation studies

The loss in selectivity due to MeCMA and CMA degradation was examined. These reactions were performed in the absence of ethylene or a catalyst and the results are given in Table 2 and Fig. S17, S18.† The results are consistent with a previous study[16] showing that the CMA stability is compromised in GVL as 25 mol% of the starting material is degraded after 8 h at 180 °C (Table 2, entry 1). Identical tests in 1,4-dioxane showed that both CMA and MeCMA were significantly more stable with only 3 mol% of MeCMA and 10 mol% of CMA being converted (Table 2, entries 3 and 4). This observation demonstrated that not only the solvent but also the state of the starting substrate (acid *vs.* ester) impact the stability of the 2-pyrone. Given the observed selectivity loss (Table 1, entries 2, 3 and 6) it appears that CMA breakdown occurs concomitantly while forming **2**, thus, impacting the global yield of the desired aromatic product.

In a previous study, it was shown that the presence of small amounts of water accelerated CMA degradation.[16] A similar water mediated breakdown was observed by Chia *et al.* when the 2-pyrone, triacetic acid lactone (TAL), was exposed to water and heat.[30] They report that TAL undergoes ring-opening in the presence of water but is stable in aprotic polar solvents. To determine if the esterified 2-pyrone was more resistant to breakdown due to water, MeCMA stability experiments were also performed in 1,4-dioxane with 5 vol% of water (Table 2, entry 6). These results show that esterification did little to prevent breakdown in the presence of water, since both CMA and MeCMA were entirely consumed. Based on these observations, it is evident that the presence of water in the solvent has to be minimized to maximize the yields of the Diels–Alder reaction products.

Overall, GVL is an environmentally friendly renewable solvent with many positive characteristics such as low toxicity and biodegradability[31–33] and, as such, is a desirable solvent for the conversion of MeCMA to MeBA. However, when BA formation was targeted, the effect of GVL on CMA stability was not significant since 25 mol% of the starting material was lost most likely through a concomitant degradation pathway (Table 1, entry 2). Moreover, the high boiling point of GVL would make the product separation difficult. As such, a low boiling bio-based acetone solvent could be utilized for increased BA selectivity of 91 mol% and would be an environmentally advantaged substitute.

Table 2 Degradation of CMA and MeCMA in 1,4-dioxane

Entry	Reactant	Solvent	CMA conv. (mol%)
1	CMA	GVL	25 (ref. 16)
2	CMA	GVL + 5 vol% water	100 (ref. 16)
3	CMA	1,4-Dioxane	10
4	MeCMA	1,4-Dioxane	3
5	CMA	1,4-Dioxane + 5 vol% water	100
6	MeCMA	1,4-Dioxane + 5 vol% water	100

Reaction conditions: Temperature: 180 °C, reaction time: 8 h, starting concentration: 10 mg ml^{-1} MeCMA/CMA (**1**) in 1,4-dioxane, reaction volume: 30 ml, pressure: 500 psig N_2, and agitation: 400 rpm.

Reaction kinetics of water mediated coumalic acid breakdown

The reaction kinetics and products from the water-mediated breakdown of CMA were determined using NMR analysis with deuterated dioxane-*d*8. Dioxane, an aprotic polar solvent, was chosen as the ideal model system due to minimal by-product formation and CMA/MeCMA degradation. Moreover, fully deuterated dioxane-*d*8 was commercially available allowing the kinetic studies to be performed in a closed system (a high pressure NMR tube from Wildmad-Labglass), which simplified the product identification and quantification without further sample workup.

Different D_2O concentrations (1–5 vol%) were added to the reaction mixture to identify the CMA breakdown dependence with respect to the water concentration. The main product identified *via* ^1H NMR after a 6.4 h reaction at 171 °C with 3 vol% D_2O was 2-butenal yielding 14.5 mol% at 25.3 mol% conversion (Fig. S19†). Minimal 2-butenal was observed with 1 vol% D_2O and virtually none with 0 vol% D_2O. The rate constant for the CMA breakdown reaction was obtained from the initial conversion data (no more than 20 mol% conversion). For each D_2O concentration experiment, a pseudo-first order reaction in CMA was fit to the data. The changes with respect to water in this regime were considered negligible as the reactions were carried out in excess D_2O (*e.g.* $[D_2O]$ was about 4 times $[CMA]_o$ at 1 vol% D_2O). Fits of $\ln([CMA]_t/[CMA]_o)$ *vs.* time were linear and the observed rate constant (k_{obs}) was obtained from the slope. Interestingly, the plot of the pseudo-first order rate constants k_{obs} as a function of $[D_2O]$ revealed a second order dependence on $[D_2O]$ with an independent degradation pathway when no D_2O was added (Fig. 1). Therefore, an overall rate law for CMA degradation was expressed as:

$$r_{CMA} = -k_{obs}[CMA] = -(k_1 + k_2[D_2O]^2)[CMA] \quad (1)$$

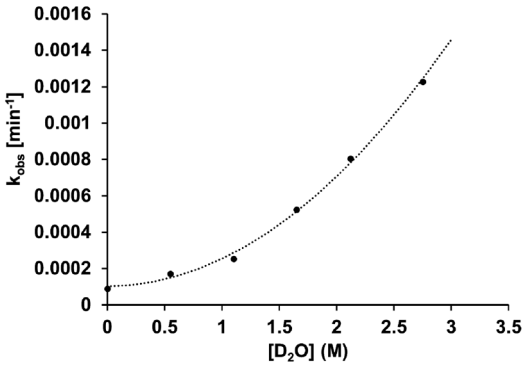

Fig. 1 Plot of k_{obs} as a function of [D_2O]. Experimentally determined k_{obs} are represented as points and the line is a simulated fit to $k_{obs} = k_1 + k_2 \times [D_2O]^2$ where $k_1 = 1.03 \times 10^{-4}$ min^{-1} and $k_2 = 1.51 \times 10^{-4}$ M^{-2} min^{-1}.

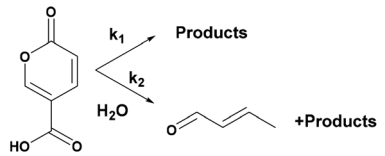

Scheme 3 General degradation of coumalic acid in the absence and presence of water.

The degradation of coumalic acid with and without the presence of water can be captured by the paths shown in Scheme 3. Further insights into the steps and mechanisms responsible for the degradation of CMA to 2-butenal were established by carrying out density functional theory calculations (Scheme 4). The results suggest that water initiated degradation of CMA proceeds *via* a nucleophilic attack of water on the double bonds in CMA. The intermediate formed (**1a**) subsequently undergoes ring-opening *via* keto–enol tautomerization to form a keto intermediate (**1b**). The presence of water molecules facilitates this ring-opening by providing a hydrogen bonding network to enable rapid proton shuttling and low

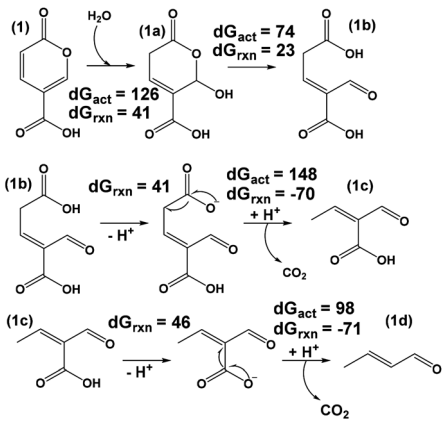

Scheme 4 CMA breakdown mechanism to 2-butenal in the presence of water (units in kJ mol^{-1}).

energy paths for keto–enol tautomerization and ring-opening. The intermediate **1b** has two carboxylic groups, which can then undergo decarboxylation yielding 2-butenal. This is very similar to a previously reported mechanism for water catalysed ring-opening and decarboxylation of triacetic acid lactone.[29]

To further validate whether CMA breakdown is solely responsible for the observed selectivity loss (Table 1, entries 2, 3 and 6) or is a result of by-product formation on the pathway to BA, the rate constants of CMA breakdown and CMA Diels–Alder addition with ethylene were compared. Based on the rate constants provided in Fig. 1 and calculated from the Diels–Alder reaction step (Table S4†), it is evident that the CMA degradation proceeds significantly slower (>100 times) than the Diels–Alder addition step. Therefore, the observed loss in product selectivity less likely originates from 2-pyrone breakdown as opposed to by-product formation from intermediates on the pathway to BA. This was further supported by DFT calculations which predicted that the Gibbs free energy of the activation barrier for water addition (126 kJ mol^{-1}) was ~15 kJ mol^{-1} higher than ethylene addition (111 kJ mol^{-1}). The increase in the barrier is likely due to hydrogen bonding stabilization of the reactant by water. Moreover, the Gibbs free energy of the reaction for ethylene addition (−79 kJ mol^{-1}) was calculated to be much more exothermic than that for water addition (41 kJ mol^{-1}) suggesting that the Diels–Alder adduct is thermodynamically favoured over CMA decomposition. Therefore, it appears that the selectivity loss of 24 mol% originates from intermediates **2** or **3** on the pathway to BA when reacting CMA with ethylene in GVL (Table 1, entry 2).

Given that reactions performed in dry polar aprotic solvents resulted in selectivities >90 mol% (with <10 mol% known by-products **4** and **6**), it appears that residual water in GVL is responsible for the selectivity loss likely from intermediate **2** or **3**. To test this hypothesis, reactions of **2** were performed *in situ* (NMR tubes) in dioxane-*d*8 at 180 °C for 4 h in the presence of 5 vol% D_2O and without a catalyst. The results from these experiments suggest that species in the ^{1}H-NMR spectra are primarily attributed to unidentified by-products that originate from either (**2**) or (**3**) on the pathway to (**5**) when water is present. From this observation, it is clearly critical to avoid water in the system to maximize the product yield by minimizing by-product formation from the reactive intermediates.

Reaction kinetics in the absence of catalyst

Kinetics measurements were performed in 1,4-dioxane which is an excellent model solvent for detailed kinetic analyses as it has a low boiling point, results in minimal by-product formation during reaction and is readily available commercially in the fully deuterated dioxane-*d*8 form to perform complementary *in situ* NMR analysis. Choosing a solvent with a low boiling point (compared to GVL) was critical for isolation, identification and quantification (*via* NMR) of the temperature sensitive reactant CMA (**1**) and intermediates **2** and **3** for both the Diels–Alder and decarboxylation reactions. The fully resolved spectra of the formation of **2** and **3** are depicted in

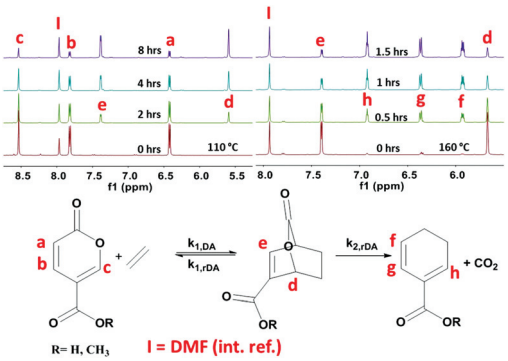

Fig. 2 NMR trace of the Diels–Alder and decarboxylation reactions.

Fig. 2 showing that the peak assignments and the method of quantification *via* NMR were unambiguous with carbon balances of >96 mol%.

Diels–Alder reaction step

The activation barrier associated with the formation of the Diels–Alder (DA) adduct (**2**) was investigated by comparing the rate of consumption of CMA at temperatures ranging from 90 to 120 °C. Under these conditions, the cycloadduct was formed in high yields without the breakdown of CMA simplifying the examination of the kinetics of this single step. The net rate of cycloadduct formation can be written as the forward rate of cycloaddition formation *via* the Diels–Alder reaction between CMA and ethylene minus the rate of the back reaction involving the retro Diels–Alder (rDA) of the cycloadduct. Assuming that both these reactions are elementary, the net rate can be written as that in eqn (2). This equation can be simplified (eqn (3)) based on the experimental conditions since ethylene was in ~10× excess, which was validated by the plots of $\ln([\mathrm{CMA}]_t/[\mathrm{CMA}]_0)$ *versus* time all giving linear relationships (Fig. S20 and S21† (MeCMA)). The experimental results and spectra (Fig. 2) suggested that the rDA reaction had only a minimal contribution as **2** can be obtained with yields of 98 mol%, which further showed that $k_{1,\mathrm{DA}} \gg k_{1,\mathrm{rDA}}$ and justified the simplification of eqn (3) into (4). DFT calculations also fully support this since ethylene addition is predicted to be highly exothermic (−127 kJ mol^{-1}).

$$-r_{\mathrm{CMA}} = k_{1,\mathrm{DA}}[\mathrm{CMA}][\mathrm{Ethylene}] - k_{1,\mathrm{rDA}}[\mathrm{DAP}] \quad (2)$$

$$-r_{\mathrm{CMA}} = k'_{1,\mathrm{DA}}[\mathrm{CMA}] - k_{1,\mathrm{rDA}}[\mathrm{DAP}] \quad (3)$$

$$-r_{\mathrm{CMA}} = k'_{1,\mathrm{DA}}[\mathrm{CMA}] \quad (4)$$

The observed rate constants at temperatures in the range of 90–120 °C are given in Table S4.† The activation energy (E_A) for the Diels–Alder reaction of CMA (or MeCMA) (depicted in Fig. 3A) was calculated based on the slope of the Arrhenius plot shown in Fig. 3B and Fig. S21.† The reaction of CMA and MeCMA with ethylene resulted in a similar activation barrier of 77 kJ mol^{-1}. The experimental values were compared to the DFT-calculated barriers, which showed excellent agreement as the calculated enthalpic activation barriers were 67 and 68 kJ mol^{-1}, respectively. Therefore, the functionality (acid or ester) had negligible influence on the 2-pyrone reactivity (Table S4†). Literature reports for the cycloaddition of CMA derivatives and dienophiles with donating or withdrawing substituents report activation barriers that range from 28 (ref. 34) to 118 (ref. 21) kJ mol^{-1} when using butyl vinyl ether or methyl acrylate, respectively. Given the nature of an inverse electron demand Diels–Alder cycloaddition, dienophiles with a higher electron density from donating substituents should react more readily than dienophiles with electron withdrawing substituents.[34,35] With an activation barrier of 77 kJ mol^{-1}, the reaction of CMA

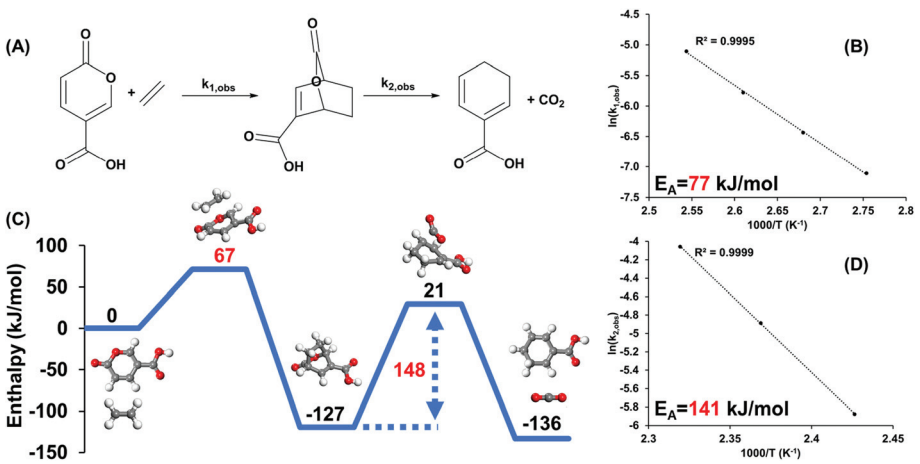

Fig. 3 Network kinetic analysis of coumalic acid reaction with ethylene. (A) Diels–Alder reaction followed by thermal CO_2 extrusion. (B) Measured activation energy of the Diels–Alder reaction of CMA and ethylene in 1,4-dioxane at temperatures between 90 and 120 °C. (C) DFT-calculated reaction energy profile diagram for the CMA reaction with ethylene to the Diels–Alder adduct followed by decarboxylation to cyclohexa-1,5-diene carboxylic acid intermediate and CO_2. (D) Measured activation energy of the thermal decarboxylation reaction of CMA-DAP in 1,4-dioxane at temperatures between 140 and 150 °C.

(MeCMA) and ethylene showed that the unactivated dienophile resulted in intermediate Diels–Alder reactivity.

Decarboxylation reaction step

Examination of the bicyclic lactone (DAP) intermediate decarboxylation was carried out at temperatures ranging from 140 to 160 °C. The reactant, intermediate **2**, was prepared using a 16 h reaction at 110 °C in 1,4-dioxane, which yielded almost pure DAP (**2**) with only trace amounts of intermediate **3** and unreacted **1**. Decarboxylation reactions were performed using high pressure Wilmad-Labglass NMR tubes. The synthesized DAP (**2**) was dissolved in dioxane-*d*8 within the tubes and the decarboxylation reactions as a function of time was measured *via* NMR (Fig. 2).

The rate law for the decarboxylation step was assumed to follow unimolecular first order kinetics (eqn (5)).

$$-r_{\mathrm{DAP}} = k_{2,\mathrm{rDA}}[\mathrm{DAP}] \quad (5)$$

During the decarboxylation reactions, no accumulation of CMA (or MeCMA) was observed at any of the temperatures tested, which provided additional support that $k_{1,\mathrm{DA}} \gg k_{1,\mathrm{rDA}}$ and helped in validating the assumption that the equilibrium between CMA (or MeCMA) and DAP (**2**) was strongly shifted towards DAP formation. Plots of $\ln([\mathrm{DAP}]_t/[\mathrm{DAP}]_0)$ *vs.* time resulted in linear trends for all temperatures tested (Fig. S22 and 23†).

The activation barriers for the decarboxylation of CMA/MeCMA-derived (**2**) (142/133 kJ mol^{-1}) were calculated based on the slope of the Arrhenius plots (Fig. 3D and Fig. S22†) using the observed rate constants (Table S5†). DFT calculations predicted an enthalpic activation barrier of 148 kJ mol^{-1} for both bicyclic lactones (CMA-DAP and MeCMA-DAP) as shown in Fig. 3C. The DFT barriers agree well with those from experiments. Abdullahi *et al.* reported that the decarboxylation of the bicyclic lactone formed from ethyl coumalate and butyl vinyl ether also results in a high activation barrier of 111 kJ mol^{-1} which is also in close agreement with the DFT results that give a CO_2 extrusion barrier of 120 kJ mol^{-1}.[36] By comparing these results with our experimental activation energy, it is evident that the decarboxylation step is significantly influenced by the degree of functionalization of the bicyclic lactone intermediate. DFT energy mapping calculations (Fig. 4) further suggested a mechanism where the CO_2-bridge leaves in an asynchronous fashion with a significantly elongated C–O bond in the transition state. As such, the C–O bond cleavage occurs prior to the C–C bond cleavage, which is in agreement with observations from the literature.[36]

From this analysis we conclude that the rate-limiting step in this reaction network is the decarboxylation reaction of **2**. We observed that all reactions performed with a catalyst led to only minimal accumulation of **3**, suggesting that the rate of dehydrogenation of **3** is much more rapid than the rate of formation of **3**. These results provide critical insight into what should be targeted to further enhance the overall process. Clearly, finding a catalyst to reduce the activation barrier of the rate-limiting decarboxylation would allow for this reaction to be carried out under milder reaction conditions, which would improve the overall yields by reducing the extent to which by-products were formed.

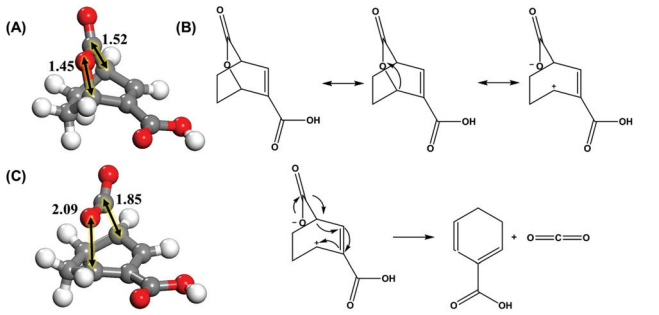

Fig. 4 Bicyclic lactone decarboxylation. (A) Bond length (Å) of the cycloadduct of CMA and ethylene. (B) The asynchronic thermal decarboxylation mechanism of the CMA/ethylene Diels–Alder adduct to cyclohexa-1,5-diene carboxylic acid. (C) Bond length (Å) of the transition state of the cycloadduct CO_2 extrusion towards the cyclohexa-1,5-diene carboxylic acid with a more advanced C–O bond cleavage.

Conclusions

In this work, we have shown that the Diels–Alder chemistry between CMA (or MeCMA) and ethylene can yield high conversion and selectivity towards BA (or MeBA), which provides a renewable alternative to current benzoate production. We were able to effectively elucidate the reaction network and revealed kinetic information such as activation energies for the Diels–Alder and the decarboxylation step. Although the CMA stability studies revealed two independent break down pathways as a function of water concentration resulting in 2-butenal as the main by-product, the CMA decomposition rate was significantly slower than the Diels–Alder cycloaddition indicating that the CMA stability is not a contributing factor. Instead, we have shown that the selectivity loss is a result of the formation of **4** and **6** and that in the presence of water intermediates on the pathway to BA led to by-product generation. Thus, the avoidance of water is critical to improve the overall selectivity. Utilizing MeCMA led to a reduction in by-product formation, consequently improving the benzoate selectivity.

Kinetic studies revealed that the activation barrier of the decarboxylation reaction was considerably higher than that of the Diels–Alder reaction, giving evidence that the extrusion of CO_2 is the rate limiting step, which is in agreement with DFT results. The high activation barrier of the CO_2 extrusion afforded the successful isolation of **2**, granting access to bicyclic molecules in high yield and selectivity that could be utilized as synthetic starting substrates to synthesize a broad array of new compounds. For instance, we have shown that diene intermediates (**3**) can be obtained from bicyclic lactones (**2**) through controlled thermal extrusion of CO_2, providing access to novel molecules with dual-functionality. These

insights can be leveraged to produce a plethora of products based on the coumalate conversion platform.

Experimental

Reagents and materials

Coumalic acid (>97%), γ-valerolactone (98%), and 10 wt% Pd on activated carbon were obtained from Sigma Aldrich. Toluene (99.9%), methanol (MS grade), water (MS grade), and acetic acid (MS grade) were obtained from Fischer Scientific. Methyl coumalate (98%) and ethylene (99.5%) were obtained from Acros Organics and Matheson, respectively. The deuterated solvents benzene-*d*6 (99.5%) and dioxane-*d*8 (99.5%) were obtained from Cambridge Isotope Laboratories Inc. All chemicals were used without further purification.

Apparatus and the general procedure

Reaction kinetics measurements for the overall reaction of CMA (or MeCMA) and ethylene were performed using a 50 ml micro reactor system from Parr (4590 Series). Catalytic reactions were carried out using a 10 wt% Pd/C catalyst, which was added to the CMA (or MeCMA) containing solution before the reactor was sealed and purged five times with nitrogen to remove residual air. The reactor was then charged with ethylene for approximately 30 min until the saturation of ethylene in the solvent was achieved. Subsequently, the system temperature was increased to the desired reaction conditions with a heating rate of 10 K min^{-1}. Samples were periodically withdrawn from the reactor through a high pressure sampling tip tube to follow the reaction progress over time. Samples were withdrawn once the reactor reached the desired reaction temperature as the starting point reference. After the liquid phase reaction products were collected, the samples were filtered through a 0.2 micron syringe filter and analysed *via* NMR, UPLC-PDA/QDa and GC-FID/MS.

The Diels–Alder reaction evaluation of CMA or MeCMA with ethylene was performed in the temperature range of 90–120 °C without the presence of a catalyst following the reaction procedure described above. The solvent 1,4-dioxane was used due to its superior solubility in both CMA and MeCMA.

The decarboxylation reaction studies of the Diels–Alder product (DAP) decarboxylation were performed in the temperature range of 140–160 °C, using high pressure NMR tubes from Wilmad-Labglass. The reactant (**2**) for this study was synthesized *via* the Diels–Alder reaction of CMA (or MeCMA) and ethylene in 1,4-dioxane at 110 °C for 16 h giving high yield (>98%). Through evaporation (using a stream of dry air) of the solvent, the reaction product (**2**) was obtained and subsequently dissolved in dioxane-*d*8. The solution was then transferred into the high-pressure NMR tubes. Before the tube was sealed, 2.5 μl of an internal standard (dimethyl formamide, DMF) was added to perform quantitative analysis. Subsequently, the tubes were placed into a heated oil bath to initiate the decarboxylation reaction. The tubes were periodically taken out of the oil bath cooled to room temperature and the reaction products were analysed *via* ^{1}H-NMR. Performing the reaction in a deuterated solvent allowed for direct NMR sample analysis of the reaction products without further sample workup.

Reaction kinetics measurements of water mediated CMA breakdown were performed using different amounts of D_2O added to the solution comprising the deuterated solvent dioxane-*d*8 and the reactant CMA. This reaction was conducted using high pressure NMR tubes from Wilmad-LabGlass that were loaded with the reaction solution, sealed and heated without exposing the reaction solution to the gaseous reactant ethylene to exclusively investigate the stability of CMA under the reaction conditions. Here, a 0.15 M stock solution of coumalic acid and a 0.025 M solution of $DMSO_2$ (internal standard) were prepared in deuterated dioxane-*d*8. A total volume of 300 μL of stock solution was added to the high pressure NMR tubes (Wilmad-Labglass) and H_2O or D_2O was added to yield 0–5 vol%. NMR tubes were sealed and heated to 171 °C. Samples were removed and allowed to cool to room temperature prior to the collection of the ^{1}H NMR spectra.

To elucidate the reaction network of the MeCMA reaction with ethylene, 2D-NMR structural assignments were carried out using different NMR techniques such as ^{1}H-NMR, ^{1}H–^{1}H COSY, and ^{13}C–^{1}H HSQC. The products analysed *via* 2D-NMR were obtained from the reaction of MeCMA and ethylene following a 48 h reaction at 90 °C in the absence of the Pd/C catalyst.

Sample analysis

NMR sample analyses of the reaction mixtures obtained from the batch reactions were carried out using a Bruker spectrometer equipped with a 14.1 Tesla superconducting magnet. The data were acquired and processed using TOPSPIN (version 3.0) and MestReNova (version 10.0.1-14719), respectively. These samples were prepared using fully deuterated benzene-d6 or dioxane-*d*8 to reduce the solvent background and as a species for field calibration. ^{1}H spectra were acquired using a recycle delay of 1.0 s and 30° ^{1}H excitation pulse lengths. ^{1}H–^{1}H 2D plots were acquired using a COSY pulse sequence, and ^{13}C–^{1}H 2D plots were acquired using a HSQC pulse sequence.

The reaction products were also analyzed by ultra-pressure liquid chromatography (UPLC) using a Waters Acquity H-Class System equipped with a Photodiode Array (PDA) and a QDa mass detector. UPLC separation was carried out on a Waters BEH phenyl column (2.1 × 100 mm, 1.7 μm particles). Additionally, the samples were analyzed by GC using an Agilent 7890B gas chromatograph equipped with an Agilent DB-1701 column (60 m × 0.25 mm), a flame ionization detector (FID), and an Agilent 5977A mass spectrometer (MS). The methyl ester versions of **1**, **3**, **4**, **5**, and **6** were verified with the NIST MS spectral library.

Computational

All of the calculations reported herein were performed using density functional theory with the M062X[37,38] hybrid functional as implemented in Gaussian 09.[39] Optimizations were

performed with a 6-311G+(d,p)[40] basis set on an ultrafine grid and tight convergence criterion for force. Solvation was modeled implicitly using the SMD model.[41] Thermal corrections and partition functions were calculated within Gaussian at 298.15 K and subsequently used to calculate enthalpy and Gibbs free energies of all species. A factor of RT ln(24.46) was added to the free energies of all species to account for a change of the reference state from 1 atm to 1 M in solution. For degradation in water, additional corrections were applied corresponding to the 55.56 M concentration of the bulk solvent.

Conflicts of interest

There are no conflicts to declare.

Acknowledgements

We gratefully acknowledge the funding from the National Science Foundation under Award EEC-0813570, the Iowa State University Chemical Instrument Facility staff members, and the Minnesota Supercomputing Institute (MSI) at the University of Minnesota. Furthermore, we would like to thank all co-workers at CBiRC for their support.

References

1 R. L. D'Ecclesia, E. Magrini, P. Montalbano and U. Triulzi, *Energy Econ.*, 2014, **46**, S11–S17.
2 E. Arceo, J. A. Ellman and R. G. Bergman, *ChemSusChem*, 2010, **3**, 811–813.
3 C. H. Christensen, J. Rass-Hansen, C. C. Marsden, E. Taarning and K. Egeblad, *ChemSusChem*, 2008, **1**, 283–289.
4 G. Fiorentino, M. Ripa and S. Ulgiati, *Biofuels, Bioprod. Biorefin.*, 2017, **11**, 195–214.
5 J. v. Haveren, E. L. Scott and J. Sanders, *Biofuels, Bioprod. Biorefin.*, 2008, **2**, 41–57.
6 K. Wagemann, *ChemBioEng Rev.*, 2015, **2**, 315–334.
7 E. Mahmoud, J. Yu, R. J. Gorte and R. F. Lobo, *ACS Catal.*, 2015, **5**, 6946–6955.
8 World Health Organisation, *Benzoic acid and Sodium benzoate. Concise international chemical assessment document*, 2000, vol. 26.
9 S. Ghosh, Y. Chisti and U. C. Banerjee, *Biotechnol. Adv.*, 2012, **30**, 1425–1431.
10 K. M. Draths, D. R. Knop and J. W. Frost, *J. Am. Chem. Soc.*, 1999, **121**, 1603–1604.
11 S. K. Green, R. E. Patet, N. Nikbin, C. L. Williams, C.-C. Chang, J. Yu, R. J. Gorte, S. Caratzoulas, W. Fan, D. G. Vlachos and P. J. Dauenhauer, *Appl. Catal., B*, 2016, **180**, 487–496.
12 J. J. Lee, G. R. Pollock Iii, D. Mitchell, L. Kasuga and G. A. Kraus, *RSC Adv.*, 2014, **4**, 45657–45664.
13 S. H. Brown, L. Bashkirova, R. Berka, T. Chandler, T. Doty, K. McCall, M. McCulloch, S. McFarland, S. Thompson and D. Yaver, *Appl. Microbiol. Biotechnol.*, 2013, **97**, 8903–8912.
14 R. M. Zelle, E. de Hulster, W. A. van Winden, P. de Waard, C. Dijkema, A. A. Winkler, J. M. Geertman, J. P. van Dijken, J. T. Pronk and A. J. van Maris, *Appl. Environ. Microbiol.*, 2008, **74**, 2766–2777.
15 S. J. Riley, Ph.D., Iowa State University, 2011.
16 T. Pfennig, R. L. Johnson and B. H. Shanks, *Green Chem.*, 2017, **19**, 3263–3271.
17 J. J. Pacheco and M. E. Davis, *Proc. Natl. Acad. Sci. U. S. A*, 2014, **111**, 8363–8367.
18 S. Bérard, C. Valle and D. Delcroix, *Ind. Eng. Chem. Res.*, 2015, **54**, 7164–7168.
19 J. J. Lee and G. A. Kraus, *Green Chem.*, 2014, **16**, 2111–2116.
20 J. J. Lee and G. A. Kraus, *Tetrahedron Lett.*, 2013, **54**, 2366–2368.
21 G. A. Kraus, G. R. Pollock Iii, C. L. Beck, K. Palmer and A. H. Winter, *RSC Adv.*, 2013, **3**, 12721–12725.
22 G. A. Kraus, S. Riley and T. Cordes, *Green Chem.*, 2011, **13**, 2734–2736.
23 I. E. Markó, G. R. Evans, P. Seres, I. Chellé and Z. Janousek, *Pure Appl. Chem.*, 1996, **68**, 113–122.
24 G. H. Posner and Y. Ishihara, *Tetrahedron Lett.*, 1994, **35**, 7545–7548.
25 N. P. Shusherina, *Russ. Chem. Rev.*, 1974, **43**, 851.
26 I. E. Markó and G. R. Evans, *Tetrahedron Lett.*, 1994, **35**, 2767–2770.
27 I. E. Markó and G. R. Evans, *Tetrahedron Lett.*, 1994, **35**, 2771–2774.
28 I. E. Markó, G. R. Evans and J.-P. Declercq, *Tetrahedron*, 1994, **50**, 4557–4574.
29 K. Afarinkia, V. Vinader, T. D. Nelson and G. H. Posner, *Tetrahedron*, 1992, **48**, 9111–9171.
30 M. Chia, M. A. Haider, G. Pollock, G. A. Kraus, M. Neurock and J. A. Dumesic, *J. Am. Chem. Soc.*, 2013, **135**, 5699–5708.
31 D. M. Alonso, S. G. Wettstein and J. A. Dumesic, *Green Chem.*, 2013, **15**, 584–595.
32 G. Strappaveccia, L. Luciani, E. Bartollini, A. Marrocchi, F. Pizzo and L. Vaccaro, *Green Chem.*, 2015, **17**, 1071–1076.
33 D. Fegyverneki, L. Orha, G. Láng and I. T. Horváth, *Tetrahedron*, 2010, **66**, 1078–1081.
34 A. Corma and H. García, *Chem. Rev.*, 2003, **103**, 4307–4366.
35 F. Fringuelli and A. Taticchi, *The Diels-Alder Reaction: Selected Practical Methods*, Wiley, 2002.
36 M. H. Abdullahi, L. M. Thompson, M. J. Bearpark, V. Vinader and K. Afarinkia, *Tetrahedron*, 2016, **72**, 6021–6024.
37 Y. Zhao and D. G. Truhlar, *J. Chem. Phys.*, 2006, **125**, 194101.
38 Y. Zhao and D. G. Truhlar, *Acc. Chem. Res.*, 2008, **41**, 157–167.
39 M. J. Frisch, G. W. Trucks, H. B. Schlegel, G. E. Scuseria, M. A. Robb, J. R. Cheeseman, G. Scalmani, V. Barone, B. Mennucci, G. A. Petersson, H. Nakatsuji, M. Caricato, X. Li, H. P. Hratchian, A. F. Izmaylov, J. Bloino, G. Zheng, J. L. Sonnenberg, M. Hada, M. Ehara, K. Toyota, R. Fukuda,

J. Hasegawa, M. Ishida, T. Nakajima, Y. Honda, O. Kitao, H. Nakai, T. Vreven, J. A. Montgomery, Jr., J. E. Peralta, F. Ogliaro, M. Bearpark, J. J. Heyd, E. Brothers, K. N. Kudin, V. N. Staroverov, R. Kobayashi, J. Normand, K. Raghavachari, A. Rendell, J. C. Burant, S. S. Iyengar, J. Tomasi, M. Cossi, N. Rega, J. M. Millam, M. Klene, J. E. Knox, J. B. Cross, V. Bakken, C. Adamo, J. Jaramillo, R. Gomperts, R. E. Stratmann, O. Yazyev, A. J. Austin, R. Cammi, C. Pomelli, J. W. Ochterski, R. L. Martin, K. Morokuma, V. G. Zakrzewski, G. A. Voth, P. Salvador, J. J. Dannenberg, S. Dapprich, A. D. Daniels, O. Farkas, J. B. Foresman, J. V. Ortiz, J. Cioslowski and D. J. Fox, *Gaussian 09, Revision A.02*, Gaussian, Inc., Wallingford CT, 2016.

40 M. J. Frisch, J. A. Pople and J. S. Binkley, *J. Chem. Phys.*, 1984, **80**, 3265–3269.

41 A. V. Marenich, C. J. Cramer and D. G. Truhlar, *J. Phys. Chem. B*, 2009, **113**, 6378–6396.